



OIST

OKINAWA INSTITUTE OF SCIENCE AND TECHNOLOGY GRADUATE UNIVERSITY  
沖縄科学技術大学院大学

## Binding of single-mutant epidermal growth factor (EGF) ligands alters the stability of the EGF receptor dimer and promotes growth signaling

Author	Stefano Pascarelli, Dalmira Merzhakupova, Gen-Ichiro Uechi, Paola Laurino
journal or publication title	Journal of Biological Chemistry
volume	297
number	1
page range	100872
year	2021-06-11
Publisher	Elsevier Inc on behalf of American Society for Biochemistry and Molecular Biology
Rights	(C) 2021 The Author(s).
Author's flag	publisher
URL	<a href="http://id.nii.ac.jp/1394/00001986/">http://id.nii.ac.jp/1394/00001986/</a>

doi: [info:doi/10.1016/j.jbc.2021.100872](https://doi.org/10.1016/j.jbc.2021.100872)



# Binding of single-mutant epidermal growth factor (EGF) ligands alters the stability of the EGF receptor dimer and promotes growth signaling

Received for publication, April 14, 2021, and in revised form, June 3, 2021 Published, Papers in Press, June 11, 2021,

<https://doi.org/10.1016/j.jbc.2021.100872>

Stefano Pascarelli<sup>1</sup>, Dalmira Merzhakupova<sup>1</sup>, Gen-Ichiro Uechi, and Paola Laurino<sup>\*1</sup>

From the Protein Engineering and Evolution Unit, Okinawa Institute of Science and Technology Graduate University, Onna, Okinawa, Japan

Edited by Roger Colbran

The epidermal growth factor receptor (EGFR) is a membrane-anchored tyrosine kinase that is able to selectively respond to multiple extracellular stimuli. Previous studies have indicated that the modularity of this system may be caused by ligand-induced differences in the stability of the receptor dimer. However, this hypothesis has not been explored using single-mutant ligands thus far. Herein, we developed a new approach to identify residues responsible for functional divergence by selecting residues in the epidermal growth factor (EGF) ligand that are conserved among orthologs yet divergent between paralogs. Then, we mutated these residues and assessed the mutants' effects on the receptor using a combination of molecular dynamics (MD) and biochemical techniques. Although the EGF mutants had binding affinities for the EGFR comparable with the WT ligand, the EGF mutants showed differential patterns of receptor phosphorylation and cell growth in multiple cell lines. The MD simulations of the EGF mutants indicated that mutations had long-range effects on the receptor dimer interface. This study shows for the first time that a single mutation in the EGF is sufficient to alter the activation of the EGFR signaling pathway at the cellular level. These results also support that biased ligand–receptor signaling in the tyrosine kinase receptor system can lead to differential downstream outcomes and demonstrate a promising new method to study ligand–receptor interactions.

The epidermal growth factor (EGF)-like domain ligand–receptor signaling system is involved in many biological events in multicellular organisms (1). This system is constituted by one receptor (epidermal growth factor receptor [EGFR]) and seven distinct peptide ligands (EGF; heparin-binding epidermal growth factor [HBEGF]; epigen [EPGN]; betacellulin [BTC]; epiregulin [EREG]; amphiregulin [AREG]; transforming growth factor- $\alpha$  [TGFA]). Upon binding to the receptor, these ligands can activate multiple intracellular downstream pathways through a network of intramolecular interactions with several feedback loops (2). For all ligands, binding induces a transition in the EGFR from monomer or

inactive dimer to an active dimer state (3, 4). However, different ligands are able to promote divergent outcomes, even at saturating concentrations; thus, the mechanism responsible of the modular downstream pathway activation is independent of ligand affinity or potency and likely encompasses intrinsic effects (5). It is well known that the EGFR system plays a key role in cancer development. In particular, some studies have shown that overexpression of the EGFR or its ligands may induce different types of cancer (6). A better understanding of the interaction between the EGFR and its ligands could lead to the development of targeted therapies (7).

Protein–protein interactions, such as that between the EGFR and its ligands, are well-studied examples of molecular coevolution in biological systems. These interactions are sometimes defined by one part (receptor) that binds several counterparts (ligands). In these instances, receptors and ligands experience different selective constraints, where receptors tend to evolve more slowly because of the necessity of binding multiple ligands (8). Furthermore, paralogs, proteins related by a duplication event, are less likely to retain the same function as orthologs, proteins related by a speciation event (9). Then, the paralogous ligands rather than the receptor are a good candidate to test the functional divergence in the biased signaling system. However, this approach is susceptible to indirect factors, such as different ligand binding selectivity, thus resulting in the activation of unrelated pathways. In this work, we decided to test single mutants of one ligand, EGF, by identifying and modifying sites responsible for a divergent function among paralog ligands. Recent studies have shown that some EGF residues such as Arg-41 and Leu-47 are highly conserved and important for high binding affinity to the EGFR (10). Another study highlighted Tyr-13, Leu-15, and His-16 in the EGF as essential for downstream activity of ErbB1 (11). These outcomes were based on structural analyses of ligands and experimental validation. Although bioinformatic tools such as contact prediction (12) or molecular dynamics (MD) (13) can give a good overall picture of ligand–receptor interactions, the contribution of single ligand residues to the modularity of the system still remains unclear.

Ligand-induced selective activation of downstream pathway has been observed in G protein–coupled receptors, a

\* For correspondence: Paola Laurino, [paola.laurino@oist.jp](mailto:paola.laurino@oist.jp).

## EGF mutants elucidate receptor transduction

phenomenon known as “biased signaling” (14, 15). A recent report hints that this mechanism might also take place in the EGFR tyrosine kinase (16). Initially, the main contributor to the modularity of the system was thought to be the affinity of the ligands to the receptor. However, the discovery of the ligand EPGN, which induces a potent mitogen effect despite low binding affinity (17), and multiple cell line studies (5) have changed this perspective. A plausible explanation was initially formulated by Wilson *et al.* (5), where different EGFR ligands induce different receptor dimer stabilities, altering the phosphorylation dynamics. Later, new experimental evidence supported this theory by observing a transient activation in stable receptor dimers induced by the EGF, whereas the activation of the weak receptor dimer induced by EPGN or EREG persisted for a longer time (18). A difference in dimer stabilities could result in alterations of the receptor oligomerization state, previously shown as a determinant of the intracellular kinase phosphorylation pattern (19). Now, the open question is how these ligands induce different dimer stabilities. Interactions between the interface of the ligand and the EGFR have been shown to influence the stability of the dimerized receptor (20), a factor that is related to ligand-specific signaling bias (18, 21). It is known that the EGFR dimer can be observed in a symmetrical, “flush” conformation or an asymmetrical, “staggered” conformation (22), depending on the presence/absence of the membrane, glycosylation, and the number of bound ligands (23). Whether and how this plays a role in biased signaling is still unknown.

Here, we show how single amino acid substitutions on the ligands effect the biased signaling in the EGF–EGFR ligand–receptor system. We developed a new bioinformatic tool to analyze the coevolution of the ligand–receptor pair and identify candidate function-altering mutations. The identified mutants induced an altered phosphorylation dynamics and different cellular phenotype (Fig. 1). This is the first study to explain differences in biased signaling of the EGFR using single-residue EGF mutants. Furthermore, our coevolutionary analysis can be applied readily to other ligand–receptor interactions.

## Results

### DIRpred

First, we developed a method for predicting residues that are likely to be responsible for functional divergence among paralogs sharing a common interactor (referred as ligands and receptor from now on). We called the method DIRpred (divergence-inducing residue prediction). Our approach combines residue-specific conservation measures to identify positions that are conserved among orthologs while diverging among paralogs. The DIRpred analysis is based on the assumption that conservation of a residue in orthologs of a specific ligand shows whether a residue is important for either structural or functional reasons, while conservation of a residue among paralogous ligands denotes the importance of a residue for interaction with the common interactor (the main shared property of all ligands). Thus, residues that are highly

conserved in orthologs but not in paralogs of a ligand are likely related to the ligand’s specific function. Unlike other existing methods for prediction of specificity determining residues (a review can be found in (24)), we included interprotein coevolution measures to narrow down those residues that are responsible for a specific interaction. The DIRpred score is calculated as the sum of the four components (I: orthologs conservation, II: complement of the paralog’s conservation, III: ligand–receptor coevolution, and IV: complement of ligand internal coevolution). Optionally, the analysis can be conducted using a structural alignment of the paralogs (multiple structural alignment [MSTA]) instead of the multiple sequence alignment (MSA). An implementation of the DIRpred analysis was done using Python. The pipeline accepts multiple sequence or structure alignments and a reference protein to conduct the analysis. The output consists of a single tabular file containing the four individual scores and the combined prediction score for each protein site, and a plotted recap of the results (Fig. S1).

### DIRpred analysis of the EGF

We applied the DIRpred algorithm to predict the residues in the EGF that induce functional divergence among paralogs (Fig. 2). Because the analysis requires prior knowledge of paralogs and orthologs of the target gene, we first performed a phylogenetic analysis to confirm that the reported paralogous ligands of the EGF are monophyletic (Fig. S2). The same tree was used in the statistical validation of the individual DIRpred scores. A random 53–amino acid–long sequence was evolved 100 times on the EGFR ligand phylogenetic tree using Pvolve (25). Assuming that the distribution of DIRpred scores will be normal, we estimated the probability that a site without functional constraints would have the same or higher than observed score (*p*-value) (26). We included the results of the statistical analysis to the output of DIRpred for the EGF (Fig. S3, Table S1). The analysis highlighted residue Asn-32, Asp-46, Lys-48, and Trp-50 as potential candidates for paralog functional divergence. Asn-32 and Lys-48 show a very small conservation in both sequence and structure alignments resulting in a high partial score (II). Asp-46 has a relatively high coevolution with the receptor (III), while Trp-50 has high scores overall (Fig. S4).

Three of the four positions were mentioned in previous reports; however, none of them was individually mutated. The tryptophan in position 50 is a strong outlier in our bioinformatics analysis, along with Trp-49 (Fig. 2). Their score is high even when using conservation measures that do not take amino acid type change into account (data not shown). However, Trp-50 was a better candidate for testing because of its outward-facing position, while Trp-49 is involved in buried protein contacts (27). Trp-49 and Trp-50 could be responsible in facilitating the interaction of the EGF with the membrane phospholipids, as it happens for Pro-7 and Leu-8 (28); Trp-49 and Trp-50 are not burying inside the bilayer when the EGF and a membrane are in solution alone (29), although this might be different when in complex

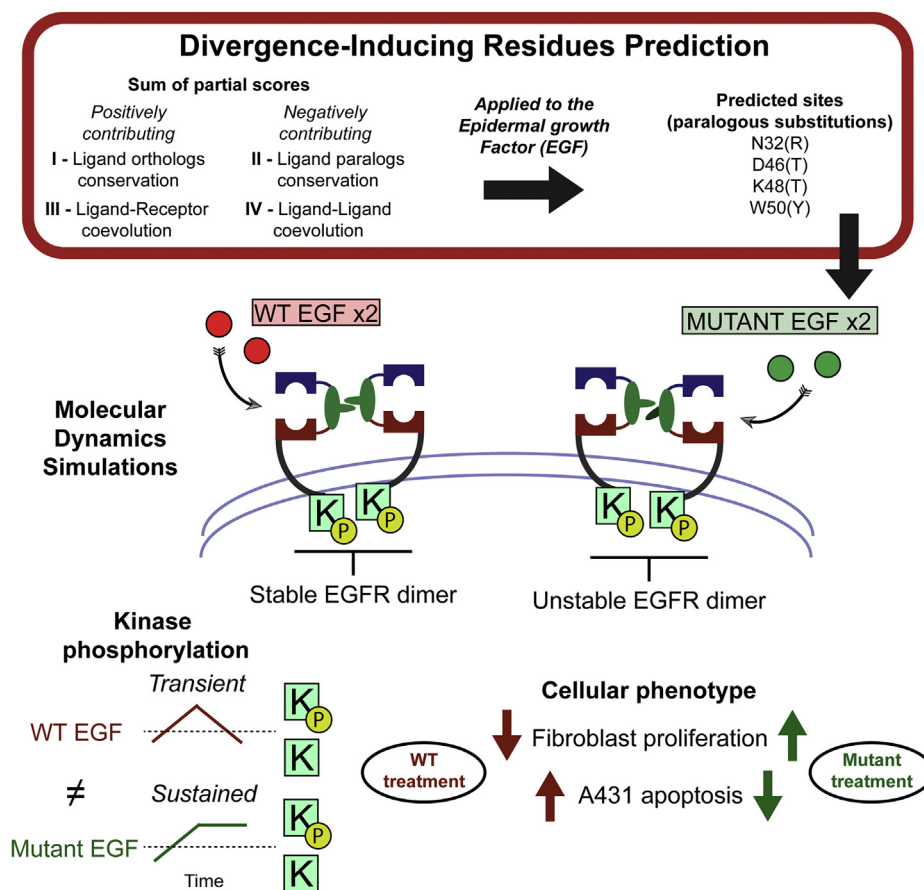


**Figure 1. Study rationale.** EGF mutants were identified using an ad hoc methodology that combines conservation and coevolution measures, DIRpred. Unlike WT EGF, the mutant ligands induce an unstable conformation of the receptor dimer, similarly to a dimer with a single WT EGF. Treating A431 and fibroblast cells with either WT EGF or mutant EGF resulted in a different response both in the phosphorylation dynamics and the cell proliferation phenotype. DIRpred, divergence-inducing residue prediction; EGF, epidermal growth factor.

with the receptor. For example, this could be achieved by Trp-50 through the formation of a helix, clustering together with Val-34 and Arg-45 around the conserved Leu-47 (30). Mutation N32R is on the interface between the ligand and receptor. The slightly higher affinity is probably due to the presence of the guanidinium group of R which is positively charged and could interact with Gln-16 of EGFR extracellular domain (ECD) (Fig. S5). Interestingly, mutations of the corresponding position in chicken transforming growth factor- $\alpha$  were able to alter the mitogenicity without strongly affecting the binding affinity (31). Although no previous literature reported about Asp-46 before, Lys-48 was found in two mutants that showed higher affinity (32).

Next, we manually chose which amino acid to introduce on the four sites depending on several factors. The main contribution to the decision was given by the paralog alignment, while also considering the amino acid type and the ligand functional divergence. The paralogs were divided into two groups based on their kinetics parameters of interaction with the receptor. After that, we selected an amino acid that infers a significant change in biochemical properties and that is found in the paralog group without the EGF. When multiple choices were possible, priority was given to the EPGN or EREG because these two

ligands are the ones observed to induce a biased signaling in the study by Freed *et al* (18). The four designed EGF mutants with a single amino-acid substitution that were selected for functional characterization are N32R, D46T, K48T, and W50Y.

### Biochemical properties of the EGF mutants

To determine the integrity of the secondary structure of the mutated ligands and the functional effects of these amino acid substitutions, we first performed *in vitro* analysis. Initially, CD spectroscopy was used to confirm that the secondary structure of the mutants was maintained (Fig. S6). The  $\beta$ -sheet content of the EGF mutants (ranging from 0.41 to 0.54 %) was not substantially different than the WT EGF (0.44%), whereas the other secondary structure varies. It is not surprising that only the beta sheet content can be detected by CD, considering that the EGF is a peptide (53 amino acids) constituted by two  $\beta$ -sheets connected by a loop and the regions at the C and N termini are flanking. Then, we tested the ability of each mutant to bind the soluble ECD of the EGFR, by isothermal titration calorimetry (ITC) and microscale thermophoresis. The mutants bound the receptor analogously to the WT sample in both the experiments



## EGF mutants elucidate receptor transduction

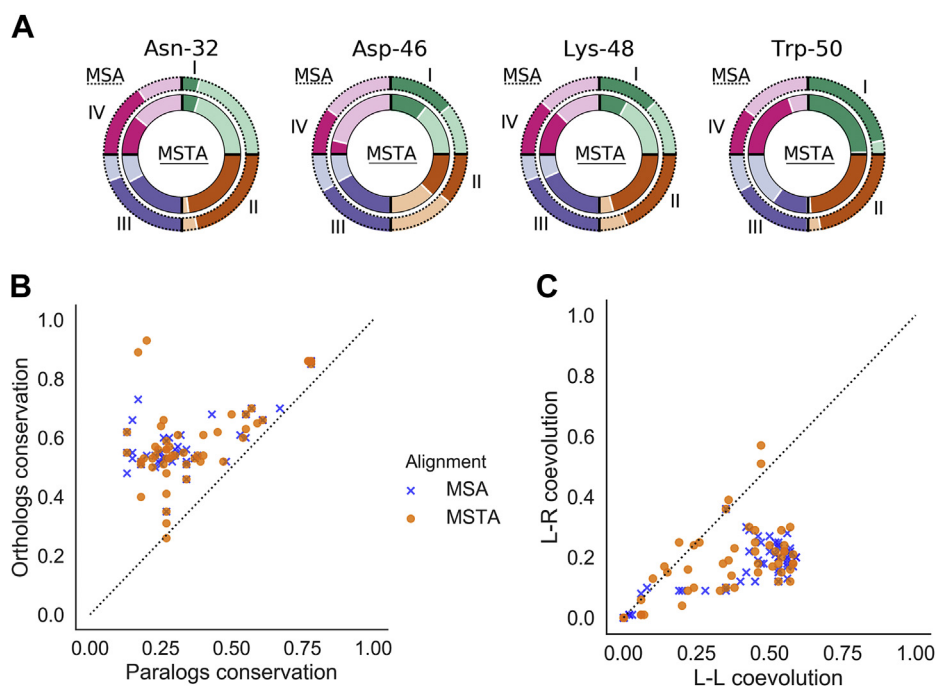


**Figure 2. DIRpred analysis of EGF.** A, the relative ranking score of the four mutants. The *outer circle* represents paralog multiple sequence analysis (MSA)-based scores, while the *inner circle* represents paralog multiple structural alignment (MSTA)-based scores. The *darker color* indicates a higher ranking in the EGF site-based scoring. The ranking values are reported in [Table S2](#). B, cross-conservation plot. The plot is obtained by crossing the two conservation scores. Interestingly, no point lies in the *bottom right* half of the plot (high paralog conservation and low ortholog conservation), suggesting that paralog and ortholog conservation is not independent. This observation points out that there is no organism-specific adaptation shared by all ligands at the protein sequence level. C, cross-coevolution score. The plot is obtained by crossing the two coevolution scores, the ligand–receptor (L-R) coevolution score (III) on the y axis and the ligand–ligand (L-L) coevolution score (IV) on the x axis. DIRpred, divergence-inducing residue prediction; EGF, epidermal growth factor.

([Fig. 3](#)). Although the N32R sample showed a slightly steeper response in both the experiments, the mutations did not appear to strongly affect the ligand secondary structure and the ability to bind the receptor.

### Biological effects of the EGF mutants

To shed light on the biological outcome of the short-term response, we sampled the effect of the EGF single mutants on EGFR expression and on the amount of phosphorylated EGFR (pEGFR) in A431 cells. A431 is a human epidermoid carcinoma cell line that overexpresses the EGFR. For this reason, we postulated that any changes at the receptor level would be amplified. We measured the amount of total and phosphorylated EGFR protein at multiple timesteps by Western blot (WB) after treating with saturating concentrations (100 nM) of WT or mutant ligands ([Fig. 4](#)). Remarkably, D46T mutant showed a reduced level of pEGFR up to 30 min after treatment ([Fig. 4A](#)). Meanwhile, the pEGFR bands for K48T and W50Y samples appear slightly stronger than the WT in the first three timesteps. However, the differences are not significant. The dimerization state of the receptor, tested by cross-linking assay, follows a similar trend as the phosphorylation experiments ([Fig. 4B](#)). After 1 h or 6 h, the treatment with the ligands also caused a reduction in the total amount of EGFR protein compared with the control ([Fig. S7](#)). However, the reduction of D46T sample did not appear as marked as the other samples. This result shows an inverse relationship between receptor activation and receptor quantity, a fact that

could be explained by the biased signaling theory. Thus, while the EGF mutants showed comparable binding affinities to the receptor, at least one of the mutants showed a different phosphorylation pattern compared with the WT ligand. Furthermore, the observed differences in the total amount of EGFR protein indicate a possible alteration in the membrane expression or recycling of the receptor.

To observe the long-term effects of the mutants on the cellular phenotype, we performed a cell growth assay using an IncuCyte live-cell analysis system on two fibroblast cell lines (Bj5- $\alpha$  and Albino Swiss mouse 3T3). With the same platform, we also performed an apoptotic assay on A431 cells by measuring the reduction in cell population, using the Annexin V green reagent to confirm the induction of apoptosis. After 1 day of initial incubation, we subjected the cells to 1, 10, or 100 nM concentration of growth factors. Treating Bj5- $\alpha$  fibroblasts with 100 nM WT EGF resulted in the highest reduction in the proliferation rate compared with the control. The reduction in proliferation was accompanied by a change in cellular morphology that could be a signal of differentiation ([Data S1](#)). However, treatment with any of the mutants decreased the ability of the ligand to suppress growth ([Fig. 5A](#)). The D46T and K48T mutants differed most from the WT ([Fig. S8A](#)). We observed a similar trend in the Albino Swiss mouse 3T3 cell line ([Fig. S8B](#)). In both cell lines, the effects are concentration dependent ([Fig. S9](#)). Next, we further tested the mutants in an apoptosis assay using the A431 cell lines. This cell line is known to exhibit apoptosis when treated with high

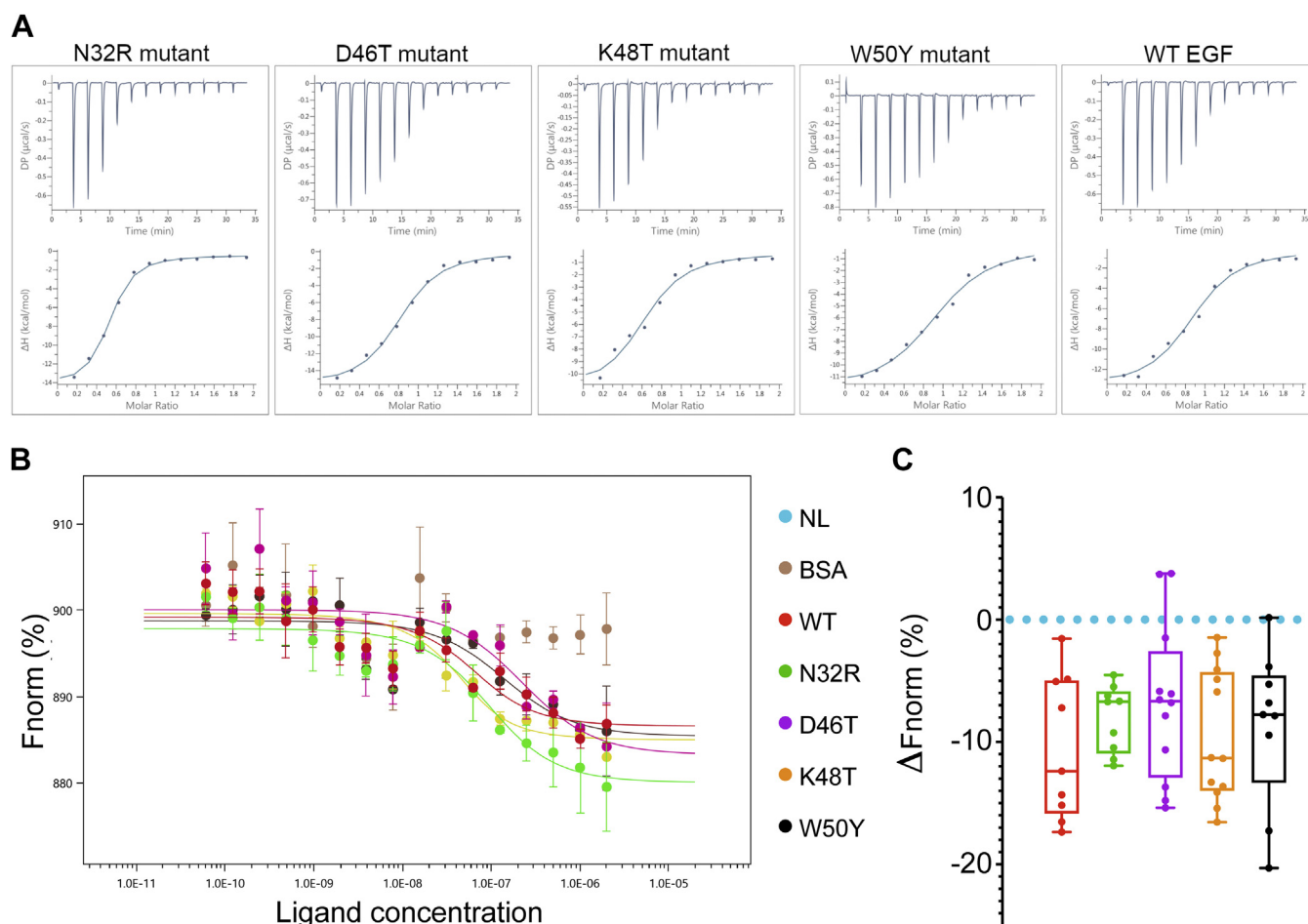


**Figure 3. Binding measurements of EGF mutants to the EGFR by isothermal titration calorimetry (ITC) and microscale thermophoresis (MST).** *A*, ITC analysis of WT EGF ligand and mutants N32R, D46T, K48T, and W50Y binding to the ECD of the EGFR at 25 °C. Measurements were taken by adding WT EGF or mutants at 200  $\mu\text{M}$  to the ECD of the EGFR at 20  $\mu\text{M}$ . *B*, extrapolated curves of the MST experiment. The normalized fluorescence difference ( $F_{\text{norm}}$ ) at 20 s for different concentrations of ligands was analyzed using the NanoTemper Technologies analysis software. Using the Kd model, it was possible to fit a curve for every sample except bovine serum albumin, which showed no binding. All ligands show a transition at about 100 nM. *C*, multiple sampling of thermophoresis was performed at a concentration of 100 nM, the point of the curve where we expected to observe a biggest difference for a ligand with an altered affinity. The  $F_{\text{norm}}$  is shown in relationship to an NL (no ligand) sample average coming from the same experimental batch. ECD, extracellular domain; EGF, epidermal growth factor; EGFR, epidermal growth factor receptor.

(>10 nM) concentrations of the EGF peptide (33). The WT showed the highest decrease in cell population 48 h after treating with 100 nM WT, while the four mutants had an intermediate response between WT and the control. Cells treated with the W50Y mutant have the closest level to the WT (Fig. 5B). In WT EGF cells, we observed evidence of apoptosis in cell's globular processes and increased ratio of Annexin to confluence signal (Fig. S10). Meanwhile, D46T- and K48T-treated cells displayed signs of cellular differentiation (Fig. 5C), in comparison with the no ligand and other mutants (Fig. S11, Data S1). Significantly, these results show that single amino acid changes in the EGF ligand display differential effects on the EGFR transduction mechanism.

The observation that the four mutations in the EGF alter signal transduction without disrupting any contacts between the ligand and the receptor can be explained by the “loss of symmetry” model of EGFR signaling (18). Freed *et al.* observed how stable symmetrical dimers show a short-lived nature of signaling, whereas asymmetric dimers conduct a sustained activation, lasting longer than 24 h. Such a model provides an

explanation on how a low level of phosphorylation after EGF treatment causes modifications in the apoptotic behavior observed in the cellular growth experiments. Compared with the WT EGF, the D46T variant shows a constantly lower phosphorylation signal, possibly through the formation of a less stable, asymmetric dimer. Thus, the observed effects of the EGF mutations on pEGFR and dimer stability are consistent with the “loss of symmetry” theory. However, the fact that some mutants have a similar phosphorylation pattern as the WT EGF but show different cellular phenotypes suggests that there might be other factors at play.

### Molecular dynamics

To understand how EGF single mutants affect the receptor signaling transduction, we performed full atomistic MD simulations of the extracellular EGFR in complex with WT or mutant ligands (100 ns each). We modeled the receptor starting from the asymmetric, “unstable” conformation of 5WB7 (22). In this way, we expected to observe a fast

## EGF mutants elucidate receptor transduction

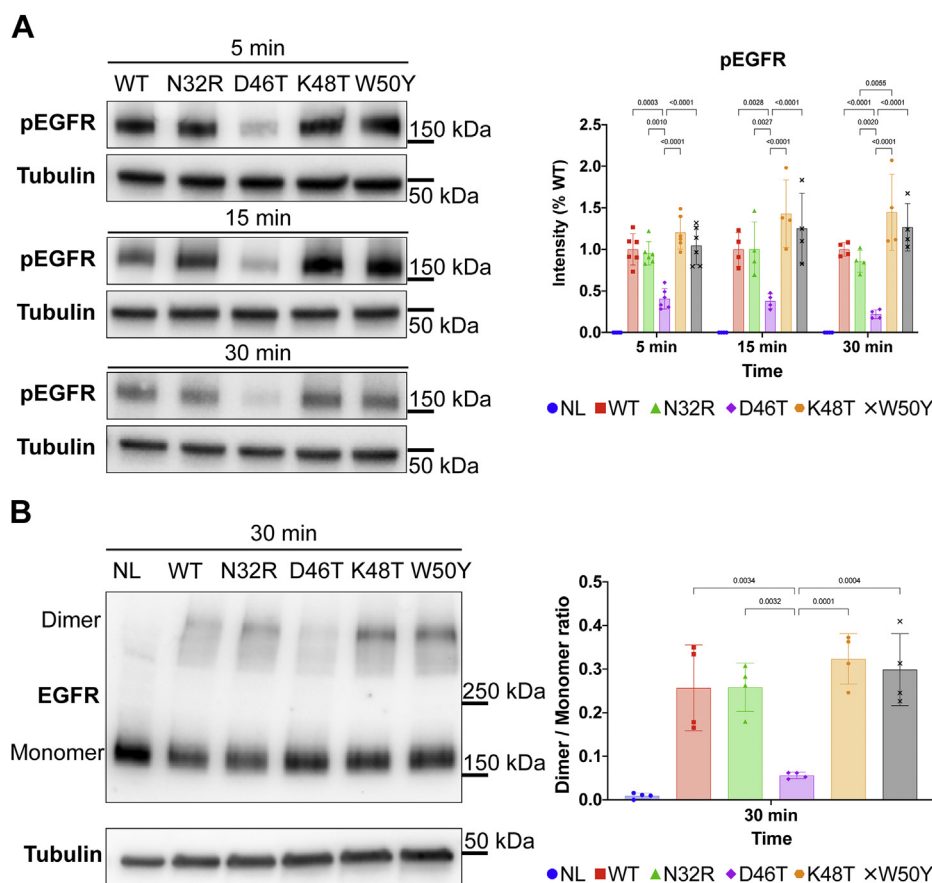


**Figure 4. Short-term response: effects of WT and single-mutant EGF on the receptor phosphorylation and dimerization in A431 cells at different time points.** *A*, short-term effects on the phosphorylation level of EGFR Tyr-1173 after treating A431 cells with 100 nM concentration of different ligands. The membrane containing the EGFR and tubulin was separated after the transfer. D46T-treated cells show a statistically significant reduction in the level of phosphorylation compared with the other samples. *B*, A431 cells were treated with 100 nM WT or mutant ligand. After 30 min, the cell lysate was run through a protocol for cross-linking and Western blot. The bars represent the mean  $\pm$  SD of at least four biological repeats. The number on top of the bars shows the *p*-values of a two-way ANOVA (*A*) or one-way ANOVA (*B*) multiple comparison corrected for multiple sampling using the Bonferroni correction. Details of the ANOVA statistics can be found in Table S3. Band intensity estimates were calculated using Bio-Rad Image Lab software (Bio-Rad). Plots and statistics were performed using PRISM software (GraphPad). EGF, epidermal growth factor; EGFR, epidermal growth factor receptor.

rearrangement for those simulations where a ligand more favorably induces a stable dimer. In previous literature, an unstable conformation was observed when removing one of the EGF ligands (23). For this reason, we also performed one simulation of the EGFR dimer in complex with only one WT ligand as a comparison (1ligEGF). The MD simulations quickly converged to a stable RMSD (Fig. 6A). For each simulation, we calculated the number of H-bonds between the two receptor dimers, and between the ligand and receptor. In the WT EGF simulation, the EGFR dimer had an average of 15 H-bonds, higher than any other simulation (Fig. 6D). However, the number of bonds between the receptor and ligand was not altered (Fig. 6E). In addition, during the course of our simulations, we also noted differences in the RMSF specifically located at the dimerization arm domain (Fig. 6B). The conformational space sampled by the dimerization arm of K48T simulation was much wider than the WT simulation (Fig. 6C). To analyze the temporal distribution of these motion, we measured the distance between Pro-272 and Gly-288 of different EGFR monomers. This distance was chosen because it was able to discriminate between the EGFR dimer in complex with EREG (PDB ID: 5WB7) and EGF (PDB ID:

1IVO). In 5WB7, one of the two distances is much bigger ( $\sim 1.10$  nm *versus* 0.4 nm) than 1IVO (Fig. 6F). In our simulations, we observe WT showing a sharp peak at 1 nm, while the mutants and 1ligEGF have a secondary peak at higher distances (Fig. 6G). Thus, the mutations in the EGF appear to affect the stability of the EGFR dimer without affecting the stability of the EGF–EGFR interaction.

## Discussion

The prediction of functional residues is a well-developed field (34), where conservation measures are considered a key factor to rely on. Tools such as ConSurf (35) and the evolutionary trace-like methods (36) are able to identify slowly evolving positions that are involved in folding, interaction, or catalytic activity (34). However, the specific reason why a residue is conserved often remains unclear. In this work, we show a new method to identify residues that affect specific functions in a system of interest. Our approach combines a conservation score calculated from the structural alignment of paralogs and among orthologs, with an intramolecular and intermolecular coevolution score with previously known



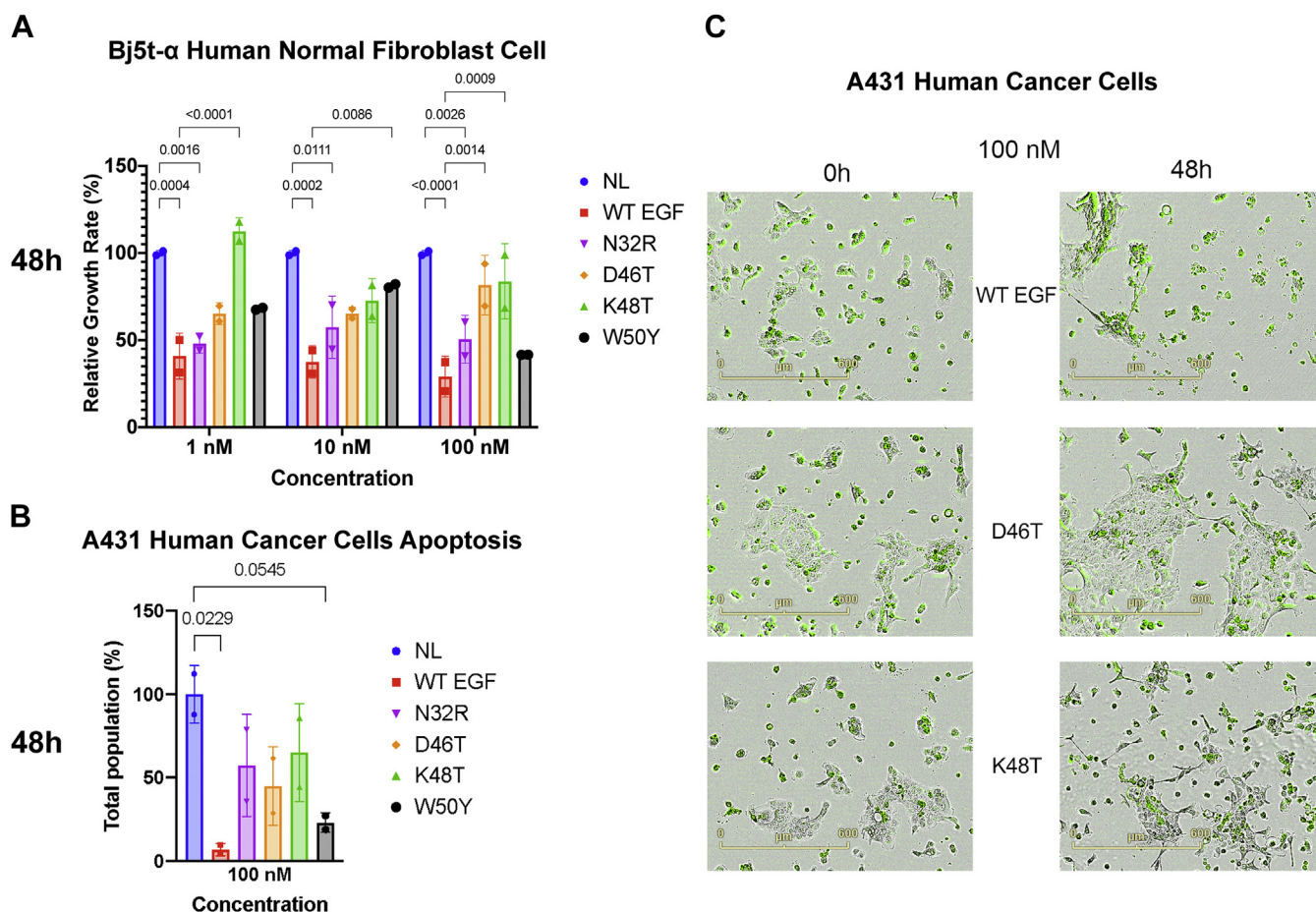


**Figure 5. Long-term response: Growth assays of cells treated with EGF variants.** *A*, effect of different concentrations of EGF variants on proliferation of the human normal fibroblast Bj5t- $\alpha$  cell line. Data represent the percentage of the growth rate, calculated from the confluence of cells, relative to the control (mean  $\pm$  SD). Percent confluence was estimated 24 h after the treatment (two replicates per treatment). *B*, apoptosis effect of WT or mutant EGF on A431 cells. EGF-induced apoptosis is measured as the reduction in total population compared with the control. *C*, comparison of A431 cell growth after treatment with 100 nM WT EGF and EGF variants D46T and K48T. Cells were labeled with fluorescent Annexin V green reagent. Plates were prewarmed before data acquisition to avoid condensation and expansion of the plate, which affect autofocus. Images were captured every 2 h (4 $\times$  magnification) for 3 days in the IncuCyte system. The number on the top of the bars shows the *p*-values of a two-way ANOVA (*A*) or one-way ANOVA (*B*) multiple comparison to the control lane, corrected for multiple sampling using the Bonferroni correction. Details of the ANOVA statistics can be found in Table S3. Band intensity estimates were calculated using Bio-Rad Image Lab software (Bio-Rad). Plots and statistics were performed using PRISM software (GraphPad). EGF, epidermal growth factor.

interactors. Conservation and coevolution give a complementary signal, thus improving the overall predictive performance (37). The coevolution score was introduced to DIRpred to highlight residues that are directly responsible of an interaction with the receptor, at the expenses of those that interact intramolecularly within the ligand. Although the first part efficiently identifies Asn-32 and Lys-48 as putative interactors, the second part does not properly give a penalty to residue Tyr-29. The interaction of this position with His-10 is also conserved in the EGF but with reversed positioning (Fig. S12), resulting in a low paralog conservation (therefore high contribution to the DIRpred score). While it is still possible to optimize the coevolution scoring function, integrating conservation and coevolution measures is a promising way to recall information of specific functions involving protein-protein interactions.

The herein studied mutations do not alter significantly the ability to bind the EGFR. However, the mutants showed a different cellular effect on Bj-5ta cells (Fig. 5). A delayed

proliferation response compared with the control might seem counterintuitive for fibroblasts (38). However, Bj-5ta hTERT immortalized fibroblasts have features that distinguish them from *in vivo* fibroblast, such as differential gene expression and EREG-dependent proliferation (39). A decrease in cell proliferation after EGF treatment could be the result of competition between the endogenously synthesized EREG and EGF, thus altering the balance between proliferation and differentiation.

A431 cells constitutionally express EGFRs at high levels. Treatment with the EGF has been observed to promote STAT1-dependent apoptosis (40). This pathway is dependent on the internalization of the ligand-receptor complex by the endocytosis process, a key factor in the ligand-induced biased signaling (16). In our experiments, A431 cells treated with mutant EGF ligands show a higher growth rate, therefore a decreased rate of apoptosis compared with the WT. Given the setting of the experiment, modularity in the endocytosis pathway is a straightforward explanation to the observed differences in the growth rate and in protein levels and phosphorylation. Interestingly, D46T- and



## EGF mutants elucidate receptor transduction

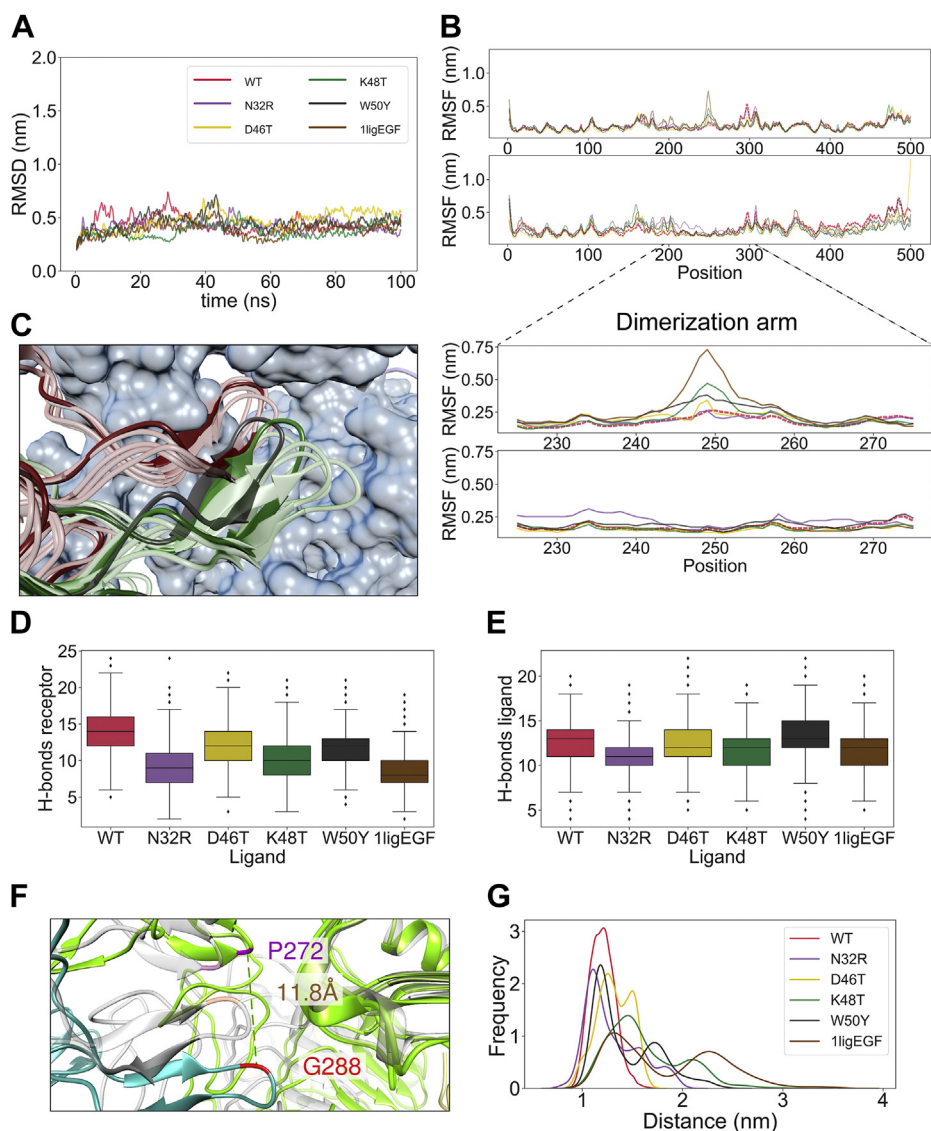


**Figure 6. Molecular dynamics of the EGFR extracellular domain.** *A*, RMSD from the initial structure. *B*, *top*, root mean square fluctuations (RMSF) of the 100-ns simulations. The WT level is marked in **bold and dashed red line**. *Bottom*, focus on the RMSF of the dimerization arm domain. The two plots represent the two EGFR in the receptor dimer. *C*, dynamics of the dimerization arm domain in WT (*red*) and K48T (*green*) simulations. A structure every 20 ns of simulation was taken and aligned to 1IVO reference structure (*blue surface and black ribbon*). The structure at 20 ns is represented in *solid colors*. K48T simulation shows a more dynamic dimerization arm. *D*, the number of H-bonds formed between the two receptors during the 100-ns simulation time. *E*, the number of H-bonds formed between the receptor that shows a dynamic dimerization arm and the corresponding ligand during the 100-ns simulation time. *F*, the distance used to investigate the fluctuations of the dimerization domain highlighted on the structure. Pro-272 (*purple*) and Gly-288 (*red*) are highlighted both on 5WB7 (*green and teal*) and in 1IVO (*gray*). The distance between the alpha carbons of the 5WB7 couple is shown in *brown* and is notably longer than 1IVO. *G*, distribution of the distance between Pro-272 and Gly-288 in all the simulations. WT simulation shows a single peak at ~1 nm, whereas in all other ligands, the distance has two peaks. EGFR, epidermal growth factor receptor.

K48T-treated cells showed an increase in long and thin cellular processes in all replicates (Fig. 5). D46T was also observed with a marked difference in the pEGFR compared with the WT (Fig. 4). A possible explanation could be the EGF-induced tubular formation, an alternative EGF-induced pathway reported in intestinal epithelial cells (41). In both the cellular growth experiments, the growth rate of the mutants is intermediate between the control and EGF, and concentration dependent. This phenomenon, and the cell line-specific response of growth hormones, is consistent with previous literature reports (42).

The analysis of the fluctuations in the dimerization arm reveals an underlying bias in ligand-induced receptor

dimerization, originally not visible from the static images of structure comparison. K48T is the mutant that induces the biggest deviation from the WT. Although, all mutants show a transition. While giving an initial outlook on the effect of the mutants, our MD simulations do not take into account other factors that could be important in the mechanism of action of the EGFR. Differential multimerization (43), oligomerization (19), receptor glycosylation, and the interaction with the membrane (23) are factors where the underlying bias induced by the mutant ligands could also have an effect in.

In this work, we showed how a single mutation of the EGF is able to alter the specific functional relationship with the

receptor. For functional divergence to arise, it could take as little as mutating 15% of the sequence (44). However, the EGFR ligands divergence date back to the vertebrate ancestor of R1/R2 whole-genome duplication, up to 500 million years ago (45), as hinted by the low (~25%) sequence identity. From our results, the sequence distance does not reflect the distance in function. In fact, the functional divergence of the EGF was altered with just a single targeted mutation.

In conclusion, our data suggests that a single mutant ligand induces a conformational change of the receptor that then affects receptor dimer stability, with plausible effects on phosphorylation level and downstream pathway activation (46). This shows how the persistence of biased signaling in the EGFR is in an unstable equilibrium, where the observed conservation of diverging sites among paralogs is naturally reinforced to maintain the functional divergence. To determine whether a short distance in function space among paralogs is a consequence or a necessity for living systems, further studies will be required.

## Experimental procedures

### Sequence and structure analysis

The sequences of EGFR ligands and the MSA of EGF orthologs were obtained from the Ensembl database (47). MSA of all ligands was performed with MAFFT software (48). X-ray structures were obtained from the PDB database (49). Structural alignments were created using Chimera (50).

### Phylogenetic analysis

From the MSA of the EGF from different species, nearly identical sequences were removed. The *Drosophila melanogaster* EGF sequence was added as an outgroup in the EGF phylogeny, while *Caenorhabditis elegans* EGF was used as outgroup for the ligand phylogeny. MSA and phylogenetic tree images were created using Unipro UGENE software (51). Three phylogenetic trees were made using the neighbor-joining, maximum likelihood, and Bayesian methods in IQ-TREE (52), using ModelFinder to scan for the best-fit evolutionary model and parameters (53).

### DIRpred

We identified sites in the EGF responsible for functional divergence using a method that combines evolutionary and coevolutionary data, called DIRpred. The DIRpred scoring function combines four components to evaluate each residue: (i) The combined conservation scores in the ortholog alignments. This score is calculated by averaging the conservation of a reference ligand site with the conservation in the respective positions of the other ligands' orthologs alignments. (ii) The complementary value ( $1 - x$ ) of the conservation score in the paralog alignment. This score can be obtained either from sequence alignment (paralog MSA) or structural alignment (paralog MSTA). (iii) The highest coevolution score between a reference ligand site and all of the receptor sites. (iv) The complementary value ( $1 - x$ ) of the highest coevolution score between a reference ligand site and all of the other ligand sites in the joint ortholog alignment of all ligands (Fig. 7).

Conservation scores were calculated using three different formulations: (1) IDENTITY, (2) BLOSUM, and (3) JSDw. The IDENTITY score measures the frequency of appearance of a reference residue in the MSA. The BLOSUM score takes the amino acid substitution frequency into account using the BLOSUM62 matrix, normalized by the maximum and minimum scores for the BLOSUM matrix. The JSDw score is based on Jensen–Shannon divergence with a window of residues (54). The FASTA sequences were imported using Biopython package, while analysis and plots were performed with Python 3 package seaborn. EGF index positions from the paralogs MSA and MSTA were, respectively, used to align the MSA- and MSTA-based scores. A schematic representation of how the four scores were obtained is shown in Figure S1.

The code used in the analysis of the DIRpred score and plots and the data used in this article are shared on GitHub: <https://github.com/oist/DIRpred>.

### Statistical validation of EGF DIRpred

The statistical analysis of EGF DIRpred scores was done as in the study by Mirny and Gelfand (55) with some modifications. The key point is that a null-hypothesis dataset should take into account the higher similarity found between orthologs, rather than between paralogs. Such a dataset was obtained through a simulated evolution performed using the Python package Pyvolve (25). The sequences in the output dataset were required to have a relationship akin to those of the EGF homologs. Using the WAG model (56), a random 53–amino acid–long protein sequence was evolved from the root of the EGF homolog tree until each leaf node, simulating a scenario of neutral evolution. Then, the sequences were divided in orthologs and paralogs using the original tree classification. The output was used as input for the DIRpred pipeline to obtain four partial scores for each site. After 100 repetitions, the partial scores were gathered together to form four background distributions. Through the assumption of normality, it was possible to estimate the probability of a site to have a higher or equal score as a randomly evolved site, that is, without functional constraints (26). The scores were considered significant only on the side where they contribute positively to the total DIRpred score, for example, when there is a lower level of paralog conservation than expected. For this reason, only one side of the normal distribution is used for the calculation of the  $p$ -value. (Fig. S3). In this way, it was possible to isolate the highly conserved cysteine positions, which usually get a misleading high overall DIRpred score. About the relative contributions of individual scores, an equal weighting system was preferred over the use of arbitrary values, which might not be always optimal. However, the pipeline allows the user to provide his own weighting system that might be more optimized for the user's study subject.

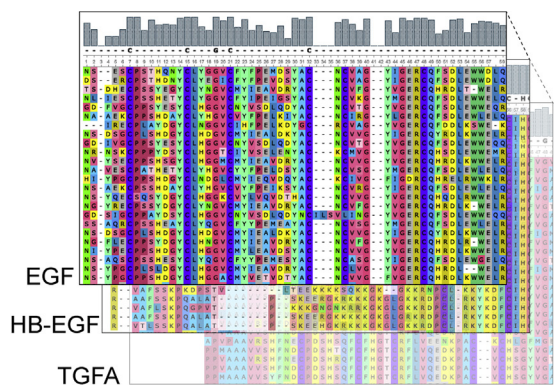
### Selection of the mutations

Along with the DIRpred score, the choice of positions for mutation was influenced by two manually curated factors: the distance from the receptor and the amino acid variation

## EGF mutants elucidate receptor transduction

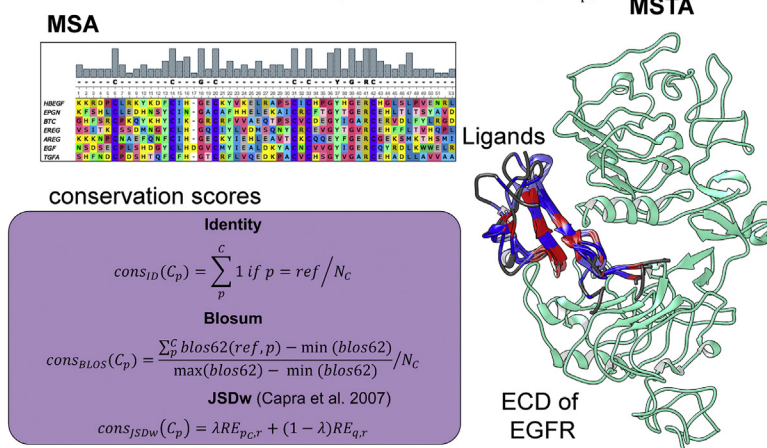
### I ) Orthologs conservation

$$I(p) = \frac{\sum_l^{para} cons\_score(l_p)}{N_l}$$



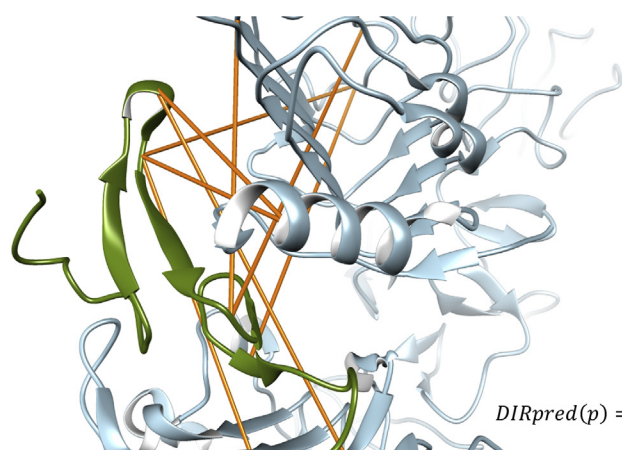
### II ) Paralogs MSA/MSTA conservation

$$II(p) = 1 - cons\_score(msa_p)$$



### III ) Ligand-receptor Co-evolution

$$III(p) = \max(coevo\_score(ref_p, EGFR_*))$$



$$DIRpred(p) = \alpha I + \beta II + \gamma III + \delta IV$$

Where

$$\alpha + \beta + \gamma + \delta = 1$$

### IV ) Ligands internal Co-evolution

$$IV(p) = 1 - \max(coevo\_score(para_p, para_*))$$

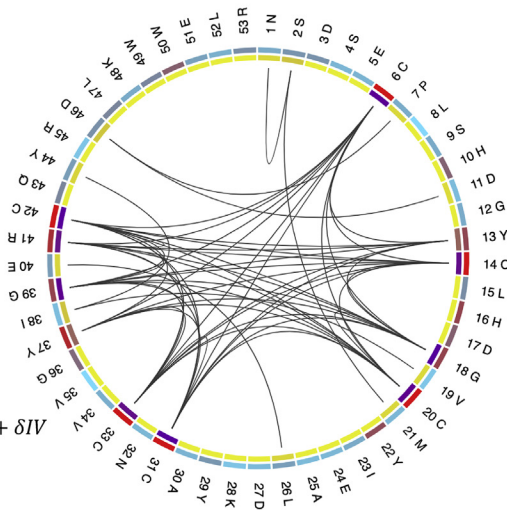


**Figure 7. DIRpred rationale.** The prediction of divergence-inducing residues consists of a linear combination of four site-specific scores, in roman numerals. In I, the ortholog MSA of each paralog is used to compute a conservation score (as exemplified from the histograms on the alignments). Alignment images were produced using Unipro software (51). In II, the human paralog sequences or structures were aligned, and the same conservation score function was used. In the purple box, the conservation score functions are represented. In III, the coevolution score between the EGF and each receptor site was computed using mutual information (MI). The yellow lines on the structure connect the highest scoring coevolving residues between the ligand and receptor. In IV, the MI coevolution score was computed from the combined ligand ortholog alignment. The circular plot was performed using MISTIC2 (72). DIRpred, divergence-inducing residue prediction; EGF, epidermal growth factor; MSA, multiple sequence alignment.

among ligand types. We designed mutations with the aim of inferring a transition to the amino acid properties in sites where the ligands show a different pattern. Overlapping residues at a given position were divided into two groups, based on an EGF-like and non-EGF-like stabilization of the receptor dimer. This property was previously shown to follow binding affinity (18). Residues that introduced a noticeable shift in amino acid properties between the two groups were selected. For example, position N32 is hydrophobic in the high-affinity ligand group, positively charged in the low-affinity group, and negatively charged in the EGF. Finally, we carefully analyzed exceptional cases in the DIRpred

scoring. Some of the residues that show a high score have intramolecular interactions with another amino acid in the ligand. These residues, if mutated, will lose EGF structural stability (namely “residue swapping” behavior shown in Fig. S12). The decision of which mutation to introduce was made using the paralog alignment, with a preferential choice over the residue found in EREG or EPGN. Positions 32, 48, and 50 have a high DIRpred score. Position 46 was included although having a lower score because the substitution pattern matches the groupings of two ligands. Furthermore, positions 46, 48, and 50 were preferred because, given previous experiments and the overall scores, the EGF C-terminal



tail seems to play a critical role in the ligand function (see, for example, (57)).

### Synthetic peptides

The WT, N32R, D46T, K48T, and W50Y variants of the EGF were ordered from Scrum Net Co with purity >90% and quantity 5 mg/ml. These peptides were used for ITC measurements, CD measurements, proliferation studies, and WB analyses.

### Cell lines

The Bj5- $\alpha$  human normal fibroblast cell line was purchased from the American Type Culture Collection. Cells were grown in Dulbecco's modified Eagle's medium (DMEM) with 10% fetal bovine serum (FBS) and 5  $\mu$ g/ml hygromycin B. The Swiss Albino 3T3 mouse normal fibroblast cell line was obtained from the RIKEN Cell Bank. Cells were grown in DMEM, 10% FBS, 50  $\mu$ g/ml gentamycin at 37 °C in a 5% CO<sub>2</sub> atmosphere with 95% humidity. The A431 human epithelial carcinoma adherent cell line (RIKEN Cell Bank) is a model skin cancer cell line with an overexpressed EGFR used for oncogenic pathway studies (58). Cells were cultured in DMEM supplemented with 10% FBS (Sigma-Aldrich), 50  $\mu$ g/ml gentamycin antibiotic or a combination of 100 unit/ml Penicillin G (Nacalai Tesque), and 100  $\mu$ g/ml streptomycin sulfate (Nacalai Tesque). Experiments were conducted at 37 °C in a 5% CO<sub>2</sub>-enriched air atmosphere with 95% humidity. Cell lines were grown and used for WB and cell proliferation studies.

### Cell proliferation assay

We measured cell proliferation using a label-free, noninvasive, cellular confluence assay with IncuCyte Live-Cell Imaging Systems (Essen BioScience). Human Bj5- $\alpha$  (2500 cells/well) and Mouse Swiss Albino 3T3 (1000 cells/well) were seeded overnight on a 96-well plate (Corning) at 37 °C in an incubator. The next day, cells were treated with WT EGF and mutants at 1 nM, 10 nM, and 100 nM concentrations and placed in an XL-3 incubation chamber maintained at 37 °C. The plate was scanned using a 4 $\times$  objective at 2-h intervals over 3 days. Cell confluence was measured using IncuCyte Analysis Software. The IncuCyte Analyzer gives real-time confluence data based on segmentation of high-definition phase-contrast images. Cell proliferation is shown as an increase in the confluence rate relative to the control.

### Apoptosis assay

Experiments were performed with the A431 human cancer cell line. 5000 cells/well were seeded on a 96-well plate (Corning) and incubated at 37 °C for 24 h. Media were replaced with fresh DMEM containing WT EGF, or EGF mutants at 1, 10, and 100 nM concentrations, and fluorescent annexin V green reagent. Plates were prewarmed before data acquisition to avoid condensation and expansion of the plate, which affect autofocus. Images were captured every 2 h (4 $\times$ ) for 3 days in the IncuCyte system. Cell proliferation is reported as in the previous assay.

### Statistics

Proliferation and apoptosis experiments were performed in duplicates. All results are shown as the mean  $\pm$  SD. Raw data were analyzed by two-way ANOVA with 95% confidence level. The multiple comparison test was corrected using the Bonferroni post hoc test. Prism 8 software was used for statistical analysis. Asterisks in the pictures show *p*-values using GraphPad convention: 0.1234 > (ns), 0.0332 > (\*), 0.0021 > (\*\*), 0.0002 > (\*\*\*), 0.0001 > (\*\*\*\*).

### Isothermal titration calorimetry

All ITC studies used a MicroCal PEAQ-ITC System (Malvern). For titration, both the EGFR ECD (Sigma-Aldrich) and EGF variants were dialyzed into the same reaction buffer Milli-Q H<sub>2</sub>O (22  $\mu$ m) at 25 °C. Each titration involved serial injections of 13  $\times$  3  $\mu$ l aliquots of EGF variants (200  $\mu$ M) into a solution of EGFR ECD (20  $\mu$ M) in the sample cell. In each case, the reference cell was filled with the same reaction buffer as the control to determine the heat upon binding of the two components. The measured heat constant value was subtracted from the heat per injection before analysis of the data. The experiment was replicated twice. Results were analyzed by MicroCal PEAQ-ITC analysis software.

### CD

Far-UV measurements were taken at a protein concentration of 0.1  $\mu$ M, using a cuvette with a path length of 0.1 cm. The secondary structure content was calculated from far-UV spectra using CAPITO software (59). Five scans in the 190- to 240-nm wavelength range were taken.

### Western blot analysis

A431 epidermoid carcinoma cells were harvested using the lysis buffer (0.4% SDS and 1 mM DTT, 1%). Samples were incubated at 37 °C for 10 min with Benzonase and centrifuged at 15,000 rpm at 22 °C for 10 min. Supernatants were used for further analysis. Sample concentrations were measured with a BCA protein assay kit (Thermo Fisher Scientific). Lysates were mixed with 4 $\times$  sample loading Laemmli buffer and incubated at 90 °C for 5 min. Equal amounts of protein were loaded in 12% Mini PROTEAN TGX SDS-PAGE gel (Bio-Rad) and transferred to PVDF membranes (Trans-Blot Turbo RTA Mini 0.2- $\mu$ m PVDF Transfer Kit). Membranes were blocked for 10 min with Bullet Blocking One (Nacalai) and reacted with monoclonal rabbit anti-EGFR antibody (Cell Signaling Technology, Inc.), Phospho-EGF Receptor (Tyr1173) (Cell Signaling Technology, Inc.), and rabbit anti- $\alpha$ -tubulin pAb (MBL) at a dilution of 1:1000. Samples were incubated with goat anti-rabbit IgG HRP at a 1:5000 dilution, and chemiluminescent signals were detected by CDP Plus (Thermo Fisher Scientific) and ChemiDoc Touch MP (Bio-Rad).

### Cross-linking assay

A431 cells were cultured in a 6-well plate to subconfluency. The cells were starved for 16 h. After activation



## EGF mutants elucidate receptor transduction

with EGF and EGF mutants for 30 min at 4 °C, the cells were washed 3 times by using ice-cold PBS. The cross-linking reaction was performed as previously reported (60). Briefly, crosslinking reagents bis(sulfosuccinimidyl) suberate (BS3) (Dojindo) were then added to a final concentration of 3.0 mM in PBS, and the reaction was incubated on ice for 15 min. The reaction was quenched by further incubation with 250 mM glycine in PBS and incubated for 15 min on ice. The cells were washed 3 times by ice-cold PBS and then lysed with 1% SDS in PBS containing proteinase inhibitor cocktail (Nacalai) on ice. The EGFR dimerization was analyzed by SDS-PAGE and Western blotting.

### Microscale thermophoresis

Recombinant human EGFR Protein (ECD, His Tag) was purchased from Sino Biological Inc. (Cosmo Bio). The protein was labeled with Large Volume His-Tag Labeling Kit RED-tris-NTA second Generation (NanoTemper) and diluted to 200 nM with 0.05% tween-PBS. EGF WT, N32R, D46T, K48T, W50Y, and bovine serum albumin were prepared by 2-fold serial dilution with 0.05% tween-PBS (4000 nM–0.122 nM). The EGFR and ligands were mixed 1:1 and incubated at room temperature for 5 min and then loaded into standard capillaries. Microscale thermophoresis measurements were performed by using Monolith NT.115 (NanoTemper).

### MD

All the simulations were performed with GROMACS version 2020 (61) using charmm36-mar2019 force field (62) and SPC216 for water. PDB ID 5wb7 was used as a model and template. EGF structure model was extracted from PDB ID livo and superimposed to the ligand using UCSF Chimera Matchmaker algorithm (63). Mutants were generated using SWISS-MODEL webserver (64), while missing atoms were compensated using Scwrl4 (65). A system was composed of the EGFR dimer in complex with one or two EGF WT, N32R, D46T, K48T, or W50Y was solvated and neutralized using NaCl ions in a dodecahedral box. Then, energy, temperature, and pressure equilibrations were performed to the system following the guidelines in the study by Lemkul, 2019 (66).

A 100-ns production simulation was run using the Verlet cut-off scheme (67) for nonbonded interactions and LINCS as the constraint algorithm (68). All the simulations reached convergence of RMSD. Long-range electrostatic interactions were computed using the Particle Mesh Ewald method (69) using a dedicated GPU. We checked for differences in relative motions between the three simulations by extracting and concatenating the backbone trajectories using catDCD plugin of VMD (70) and then performing a principal component analysis using Bio3D R package (71).

### Data availability

The source code and alignment data to reproduce the analysis of this article are available at <https://zenodo.org/>

[badge/latestdoi/287415954](https://doi.org/10.26434/chemrxiv-2021-08). All remaining data are contained within the article and [supporting information](#).

**Supporting information**—This article contains [supporting information](#).

**Acknowledgments**—We thank Tadashi Yamamoto and Ichiro Maruyama for providing the antibodies and Keiko Kono for the technical help with the WB experiments. We are grateful for the help and support provided by the Scientific Computing section of Research Support Division and in particular Jan Moren at Okinawa Institute of Science and Technology. We thank Madhuri Gade, Mirco Dindo, Harry Wilson, and Benjamin Clifton for critical reading. We thank Pierre Matricon for the discussion on the molecular dynamics data, Russel Alenton for the discussion on the cell proliferation assay, and Christine Guzman for the discussion on the Western blot analyses, and Saacnicteh Toledo Patino for the help with the NanoTemper instrument.

**Author contributions**—S. P., D. M., and P. L. conceptualization; S. P., D. M., and P. L. data curation; S. P. software; S. P., D. M., and G.-I. U. formal analysis; S. P., D. M., and G.-I. U. validation; S. P., D. M., G.-I. U., and P. L. investigation; S. P. and D. M. visualization; S. P., D. M., and G.-I. U. methodology; S. P., D. M., G.-I. U., and P. L. writing—original draft; S. P., D. M., G.-I. U., and P. L. writing—review and editing; P. L. resources; P. L. supervision; P. L. funding acquisition; P. L. project administration.

**Funding and additional information**—Financial support by the Okinawa Institute of Science and Technology to P. L. is gratefully acknowledged.

**Conflict of interest**—The authors declare that they have no conflict of interest with the contents of this article.

**Abbreviations**—The abbreviations used are: DIRpred, divergence-inducing residue prediction; ECD, extracellular domain; EGF, epidermal growth factor; EGFR, epidermal growth factor receptor; EPGN, epigen; EREG, epiregulin; FBS, fetal bovine serum; ITC, isothermal titration calorimetry; MSA, multiple sequence alignment; MSTA, multiple structural alignment; pEGFR, EGFR phosphorylation.

### References

1. Gazdar, A. F. (2009) Activating and resistance mutations of EGFR in non-small-cell lung cancer: Role in clinical response to EGFR tyrosine kinase inhibitors. *Oncogene* **28**, S24–S31
2. Oda, K., Matsuoka, Y., Funahashi, A., and Kitano, H. (2005) A comprehensive pathway map of epidermal growth factor receptor signaling. *Mol. Syst. Biol.* **1**, 2005.0010
3. Landau, M., Fleishman, S. J., and Ben-Tal, N. (2004) A putative mechanism for downregulation of the catalytic activity of the EGF receptor via direct contact between its kinase and C-terminal domains. *Structure* **12**, 2265–2275
4. Purba, E. R., Saita, E. I., and Maruyama, I. N. (2017) Activation of the EGF receptor by ligand binding and oncogenic mutations: The "Rotation model". *Cells* **6**, 13
5. Wilson, K. J., Gilmore, J. L., Foley, J., Lemmon, M. A., and Riese, D. J., 2nd. (2009) Functional selectivity of EGF family peptide growth factors: Implications for cancer. *Pharmacol. Ther.* **122**, 1–8
6. Nicholson, R. I., Gee, J. M., and Harper, M. E. (2001) EGFR and cancer prognosis. *Eur. J. Cancer* **37** Suppl 4, S9–S15

7. Xu, M. J., Johnson, D. E., and Grandis, J. R. (2017) EGFR-targeted therapies in the post-genomic era. *Cancer Metastasis Rev.* **36**, 463–473
8. Alvarez-Ponce, D., Feyertag, F., and Chakraborty, S. (2017) Position matters: Network centrality considerably impacts rates of protein evolution in the human protein-protein interaction network. *Genome Biol. Evol.* **9**, 1742–1756
9. Jensen, R. A. (2001) Orthologs and paralogs - we need to get it right. *Genome Biol.* **2**, Interactions1002
10. Groenen, L. C., Nice, E. C., and Burgess, A. W. (1994) Structure-function-relationships for the EGF/TGF- $\alpha$  family of mitogens. *Growth Factors* **11**, 235–257
11. Souriau, C., Gracy, J., Chiche, L., and Weill, M. (1999) Direct selection of EGF mutants displayed on filamentous phage using cells overexpressing EGF receptor. *Biol. Chem.* **380**, 451–458
12. Skwark, M. J., Raimondi, D., Michel, M., and Elofsson, A. (2014) Improved contact predictions using the recognition of protein like contact patterns. *PLoS Comput. Biol.* **10**, e1003889
13. Gocheva, G., and Ivanova, A. (2019) A look at receptor-ligand pairs for active-targeting drug delivery from crystallographic and molecular dynamics perspectives. *Mol. Pharm.* **16**, 3293–3321
14. Evans, B. A., Sato, M., Sarwar, M., Hutchinson, D. S., and Summers, R. J. (2010) Ligand-directed signalling at beta-adrenoceptors. *Br. J. Pharmacol.* **159**, 1022–1038
15. Kenakin, T. (2011) Functional selectivity and biased receptor signaling. *J. Pharmacol. Exp. Ther.* **336**, 296–302
16. Ali, R., Brown, W., Purdy, S. C., Davisson, V. J., and Wendt, M. K. (2018) Biased signaling downstream of epidermal growth factor receptor regulates proliferative versus apoptotic response to ligand. *Cell Death Dis.* **9**, 976
17. Strachan, L., Murison, J. G., Prestidge, R. L., Sleeman, M. A., Watson, J. D., and Kumble, K. D. (2001) Cloning and biological activity of epigen, a novel member of the epidermal growth factor superfamily. *J. Biol. Chem.* **276**, 18265–18271
18. Freed, D. M., Bessman, N. J., Kiyatkin, A., Salazar-Cavazos, E., Byrne, P. O., Moore, J. O., Valley, C. C., Ferguson, K. M., Leahy, D. J., Lidke, D. S., and Lemmon, M. A. (2017) EGFR ligands differentially stabilize receptor dimers to specify signaling kinetics. *Cell* **171**, 683–695.e618
19. Huang, Y., Bharill, S., Karandur, D., Peterson, S. M., Marita, M., Shi, X., Kaliszewski, M. J., Smith, A. W., Isacoff, E. Y., and Kuriyan, J. (2016) Molecular basis for multimerization in the activation of the epidermal growth factor receptor. *Elife* **5**, e14107
20. Mehrabi, M., Mahdiuni, H., Rasouli, H., Mansouri, K., Shahlaei, M., and Khodarahmi, R. (2018) Comparative experimental/theoretical studies on the EGFR dimerization under the effect of EGF/EGF analogues binding: Highlighting the importance of EGF/EGFR interactions at site III interface. *Int. J. Biol. Macromol.* **115**, 401–417
21. Knudsen, S. L., Mac, A. S., Henriksen, L., van Deurs, B., and Grovdal, L. M. (2014) EGFR signaling patterns are regulated by its different ligands. *Growth Factors* **32**, 155–163
22. Liu, P., Cleveland, T. E., Bouyain, S., Byrne, P. O., Longo, P. A., and Leahy, D. J. (2012) A single ligand is sufficient to activate EGFR dimers. *Proc. Natl. Acad. Sci. U. S. A.* **109**, 10861–10866
23. Arkhipov, A., Shan, Y., Kim, E. T., and Shaw, D. E. (2014) Membrane interaction of bound ligands contributes to the negative binding cooperativity of the EGF receptor. *PLoS Comput. Biol.* **10**, e1003742
24. Chagoyen, M., García-Martín, J. A., and Pazos, F. (2015) Practical analysis of specificity-determining residues in protein families. *Brief. Bioinform.* **17**, 255–261
25. Spielman, S. J., and Wilke, C. O. (2015) Pyvolve: A flexible Python module for simulating sequences along phylogenies. *PLoS One* **10**, e0139047
26. Chakrabarti, S., Bryant, S. H., and Panchenko, A. R. (2007) Functional specificity lies within the properties and evolutionary changes of amino acids. *J. Mol. Biol.* **373**, 801–810
27. Gally, J., Vincent, M., Li de la Sierra, I. M., Alvarez, J., Ubieta, R., Madrazo, J., and Padron, G. (1993) Protein flexibility and aggregation state of human epidermal growth factor. A time-resolved fluorescence study of the native protein and engineered single-tryptophan mutants. *Eur. J. Biochem.* **211**, 213–219
28. Tynan, C. J., Roberts, S. K., Rolfe, D. J., Clarke, D. T., Loeffler, H. H., Kastner, J., Winn, M. D., Parker, P. J., and Martin-Fernandez, M. L. (2011) Human epidermal growth factor receptor (EGFR) aligned on the plasma membrane adopts key features of Drosophila EGFR asymmetry. *Mol. Cell Biol.* **31**, 2241–2252
29. Li De La Sierra, I. M., Vincent, M., Padron, G., and Gally, J. (1992) Interaction of recombinant human epidermal growth factor with phospholipid vesicles. A steady-state and time-resolved fluorescence study of the bis-tryptophan sequence (TRP49-TRP50). *Eur. Biophys. J.* **21**, 337–344
30. Hommel, U., Harvey, T. S., Driscoll, P. C., and Campbell, I. D. (1992) Human epidermal growth factor. High resolution solution structure and comparison with human transforming growth factor alpha. *J. Mol. Biol.* **227**, 271–282
31. Puddicombe, S. M., Chamberlin, S. G., MacGarvie, J., Richter, A., Drummond, D. R., Collins, J., Wood, L., and Davies, D. E. (1996) The significance of valine 33 as a ligand-specific epitope of transforming growth factor alpha. *J. Biol. Chem.* **271**, 15367–15372
32. Lahti, J. L., Lui, B. H., Beck, S. E., Lee, S. S., Ly, D. P., Longaker, M. T., Yang, G. P., and Cochran, J. R. (2011) Engineered epidermal growth factor mutants with faster binding on-rates correlate with enhanced receptor activation. *FEBS Lett.* **585**, 1135–1139
33. Gulli, L. F., Palmer, K. C., Chen, Y. Q., and Reddy, K. B. (1996) Epidermal growth factor-induced apoptosis in A431 cells can be reversed by reducing the tyrosine kinase activity. *Cell Growth Differ.* **7**, 173–178
34. Nemoto, W., Saito, A., and Oikawa, H. (2013) Recent advances in functional region prediction by using structural and evolutionary information - remaining problems and future extensions. *Comput. Struct. Biotechnol. J.* **8**, e201308007
35. Ashkenazy, H., Abadi, S., Martz, E., Chay, O., Mayrose, I., Pupko, T., and Ben-Tal, N. (2016) ConSurf 2016: An improved methodology to estimate and visualize evolutionary conservation in macromolecules. *Nucleic Acids Res.* **44**, W344–W350
36. Lichtarge, O., Bourne, H. R., and Cohen, F. E. (1996) An evolutionary trace method defines binding surfaces common to protein families. *J. Mol. Biol.* **257**, 342–358
37. Teppa, E., Wilkins, A. D., Nielsen, M., and Buslje, C. M. (2012) Disentangling evolutionary signals: Conservation, specificity determining positions and coevolution. Implication for catalytic residue prediction. *BMC Bioinformatics* **13**, 235
38. Carpenter, G., and Cohen, S. (1979) Epidermal growth factor. *Annu. Rev. Biochem.* **48**, 193–216
39. Lindvall, C., Hou, M., Komurasaki, T., Zheng, C., Henriksson, M., Sedivy, J. M., Bjorkholm, M., Teh, B. T., Nordenskjold, M., and Xu, D. (2003) Molecular characterization of human telomerase reverse transcriptase-immortalized human fibroblasts by gene expression profiling: Activation of the epiregulin gene. *Cancer Res.* **63**, 1743–1747
40. Grudinkin, P. S., Zenin, V. V., Kropotov, A. V., Dorosh, V. N., and Nikolsky, N. N. (2007) EGF-induced apoptosis in A431 cells is dependent on STAT1, but not on STAT3. *Eur. J. Cell Biol.* **86**, 591–603
41. Ibuka, S., Matsumoto, S., Fujii, S., and Kikuchi, A. (2015) The P2Y(2) receptor promotes Wnt3a- and EGF-induced epithelial tubular formation by IEC6 cells by binding to integrins. *J. Cell Sci.* **128**, 2156–2168
42. Bjorkelund, H., Gedda, L., and Andersson, K. (2011) Comparing the epidermal growth factor interaction with four different cell lines: Intriguing effects imply strong dependency of cellular context. *PLoS One* **6**, e16536
43. Macdonald-Obermann, J. L., and Pike, L. J. (2014) Different epidermal growth factor (EGF) receptor ligands show distinct kinetics and biased or partial agonism for homodimer and heterodimer formation. *J. Biol. Chem.* **289**, 26178–26188
44. Zhou, J., Liu, D., Sa, Z., Huang, W., Zou, Y., and Gu, X. (2017) Effective estimation of the minimum number of amino acid residues required for functional divergence between duplicate genes. *Mol. Phylogenet. Evol.* **113**, 126–138
45. Laisney, J., Braasch, I., Walter, R. B., Meierjohann, S., and Scharl, M. (2010) Lineage-specific co-evolution of the Egf receptor/ligand signaling system. *BMC Evol. Biol.* **10**, 16

## EGF mutants elucidate receptor transduction

46. Bakker, J., Spits, M., Neeffjes, J., and Berlin, I. (2017) The EGFR odyssey – from activation to destruction in space and time. *J. Cell Sci.* **130**, 4087–4096
47. Zerbinò, D. R., Achuthan, P., Akanni, W., Amode, M. R., Barrell, D., Bhai, J., Billis, K., Cummins, C., Gall, A., Giron, C. G., Gil, L., Gordon, L., Haggerty, L., Haskell, E., Hourlier, T., et al. (2018) Ensembl 2018. *Nucleic Acids Res.* **46**, D754–D761
48. Katoh, K., and Standley, D. M. (2013) MAFFT multiple sequence alignment software version 7: Improvements in performance and usability. *Mol. Biol. Evol.* **30**, 772–780
49. Berman, H. M., Westbrook, J., Feng, Z., Gilliland, G., Bhat, T. N., Weissig, H., Shindyalov, I. N., and Bourne, P. E. (2000) The protein data bank. *Nucleic Acids Res.* **28**, 235–242
50. Goddard, T. D., Huang, C. C., Meng, E. C., Pettersen, E. F., Couch, G. S., Morris, J. H., and Ferrin, T. E. (2018) UCSF ChimeraX: Meeting modern challenges in visualization and analysis. *Protein Sci.* **27**, 14–25
51. Okonechnikov, K., Golosova, O., Fursov, M., and Team, U. (2012) Unipro UGENE: A unified bioinformatics toolkit. *Bioinformatics* **28**, 1166–1167
52. Nguyen, L. T., Schmidt, H. A., von Haeseler, A., and Minh, B. Q. (2015) IQ-TREE: A fast and effective Stochastic algorithm for estimating maximum-likelihood phylogenies. *Mol. Biol. Evol.* **32**, 268–274
53. Kalyaanamoorthy, S., Minh, B. Q., Wong, T. K. F., von Haeseler, A., and Jermiin, L. S. (2017) ModelFinder: Fast model selection for accurate phylogenetic estimates. *Nat. Methods* **14**, 587–589
54. Capra, J. A., and Singh, M. (2007) Predicting functionally important residues from sequence conservation. *Bioinformatics* **23**, 1875–1882
55. Mirny, L. A., and Gelfand, M. S. (2002) Using orthologous and paralogous proteins to identify specificity-determining residues in bacterial transcription factors. *J. Mol. Biol.* **321**, 7–20
56. Whelan, S., and Goldman, N. (2001) A general empirical model of protein evolution derived from multiple protein families using a maximum-likelihood approach. *Mol. Biol. Evol.* **18**, 691–699
57. Puddicombe, S. M., Wood, L., Chamberlin, S. G., and Davies, D. E. (1996) The interaction of an epidermal growth factor/transforming growth factor alpha tail chimera with the human epidermal growth factor receptor reveals unexpected complexities. *J. Biol. Chem.* **271**, 30392–30397
58. Giard, D. J., Aaronson, S. A., Todaro, G. J., Arnstein, P., Kersey, J. H., Dosik, H., and Parks, W. P. (1973) *In vitro* cultivation of human tumors: Establishment of cell lines derived from a series of solid tumors. *J. Natl. Cancer Inst.* **51**, 1417–1423
59. Wiedemann, C., Bellstedt, P., and Grolach, M. (2013) CAPITO—a web server-based analysis and plotting tool for circular dichroism data. *Bioinformatics* **29**, 1750–1757
60. Turk, H. F., and Chapkin, R. S. (2015) Analysis of epidermal growth factor receptor dimerization by BS<sup>3</sup> cross-linking. *Methods Mol. Biol.* **1233**, 25–34
61. Abraham, M. J., Murtola, T., Schulz, R., Páll, S., Smith, J. C., Hess, B., and Lindahl, E. (2015) Gromacs: High performance molecular simulations through multi-level parallelism from laptops to supercomputers. *SoftwareX* **1-2**, 19–25
62. Huang, J., and MacKerell, A. D., Jr. (2013) CHARMM36 all-atom additive protein force field: Validation based on comparison to NMR data. *J. Comput. Chem.* **34**, 2135–2145
63. Meng, E. C., Pettersen, E. F., Couch, G. S., Huang, C. C., and Ferrin, T. E. (2006) Tools for integrated sequence-structure analysis with UCSF Chimera. *BMC Bioinformatics* **7**, 339
64. Waterhouse, A., Bertoni, M., Bienert, S., Studer, G., Tauriello, G., Gumienny, R., Heer, F. T., de Beer, T. A. P., Rempfer, C., Bordoli, L., Lepore, R., and Schwede, T. (2018) SWISS-MODEL: Homology modelling of protein structures and complexes. *Nucleic Acids Res.* **46**, W296–W303
65. Krivov, G. G., Shapovalov, M. V., and Dunbrack, R. L., Jr. (2009) Improved prediction of protein side-chain conformations with SCRWRLA. *Proteins* **77**, 778–795
66. Lemkul, J. A. (2019) From proteins to perturbed Hamiltonians: A suite of tutorials for the GROMACS-2018 molecular simulation package [article v1.0]. *Living J. Comp. Mol. Sci.* **1**, 5068
67. Páll, S., and Hess, B. (2013) A flexible algorithm for calculating pair interactions on SIMD architectures. *Computer Phys. Commun.* **184**, 2641–2650
68. Hess, B., Bekker, H., Berendsen, H. J. C., and Fraaije, J. G. E. M. (1997) Lincs: A linear constraint solver for molecular simulations. *J. Comput. Chem.* **18**, 1463–1472
69. Essmann, U., Perera, L., Berkowitz, M. L., Darden, T., Lee, H., and Pedersen, L. G. (1995) A smooth particle mesh Ewald method. *J. Chem. Phys.* **103**, 8577–8593
70. Humphrey, W., Dalke, A., and Schulten, K. (1996) Vmd: Visual molecular dynamics. *J. Mol. Graph* **14**, 27–38
71. Grant, B. J., Rodrigues, A. P., ElSawy, K. M., McCammon, J. A., and Caves, L. S. (2006) Bio3d: an R package for the comparative analysis of protein structures. *Bioinformatics* **22**, 2695–2696
72. Colell, E. A., Iserte, J. A., Simonetti, F. L., and Marino-Buslje, C. (2018) MISTIC2: Comprehensive server to study coevolution in protein families. *Nucleic Acids Res.* **46**, W323–w328